1   **Systematic quantification of synapses in primary neuronal culture**

2   Peter Verstraelen[1]*, Gerardo Garcia[1]*, Marlies Verschuuren[1], Bob Asselbergh[2], Rony

3   Nuydens[1,3], Peter Larsen[3], Jean-Pierre Timmermans[1], Winnok H. De Vos[1]

4   [1]Laboratory of Cell Biology and Histology, University of Antwerp, Antwerp, Belgium

5   [2]VIB Center for Molecular Neurology, University of Antwerp, Belgium

6   [3]Janssen Research & Development, a Division of Janssen Pharmaceutica NV, Beerse, Belgium

7   * equal contribution

8

9   Correspondence: Prof. Dr. Winnok H. De Vos - Winnok.Devos@uantwerpen.be

10

11   **Keyword**

12   Synapse, colocalization, antibody, high-throughput microscopy, dendritic spine, image

13   analysis, proximity ligation assay, synapse density, neuron, primary neurons, screening

14

15

16 **Abstract**

17 A vast set of neurological disorders is associated with impaired synaptic connectivity.

18 Therefore, modulation of synapse formation could have therapeutic relevance. However, the

19 high density and small size of synapses make their quantification a challenging task. To

20 improve the reliability of synapse-oriented drug screens, we evaluated a panel of synapse-

21 targeting antibodies for their labeling specificity on hippocampal and cortical cell cultures using

22 quantitative immunofluorescence microscopy. For those antibodies that passed multiparametric

23 validation, we assessed pairwise colocalization, an often-used readout for established synapses.

24 We found that even when two pan-synaptic markers were used, the overlap was incomplete,

25 and the presence of spurious signals limited the dynamic range. To circumvent this problem,

26 we implemented a proximity ligation-based approach, that only leads to a signal when two pre-

27 and postsynaptic markers are sufficiently close. We demonstrate that this approach can be

28 applied to different synaptic marker combinations and can be successfully used for

29 quantification of synapse density in cultures of different maturity stage in healthy or

30 pathological conditions. Thus, the unbiased analysis of synapse labeling and exploitation of

31 resident protein proximity, allows increasing the sensitivity of synapse quantifications in

32 neuronal culture and therefore represents a valuable extension of the analytical toolset for *in*

33 *vitro* synapse screens.

34

35

Introduction

36

37 Synapses are the prime mediators of neuronal communication and their plasticity defines

38 learning and memory. They are considered to be vulnerable to many neuropathological

39 conditions. In Alzheimer's disease for instance, soluble oligomers of beta-amyloid (Aβ) and

40 hyperphosphorylated tau localize to synaptic terminals, causing their number to decline even in

41 the early stages of the disease (1-3). Synapse loss is recapitulated in mouse models that

42 overexpress human APP (4, 5) and in WT mice that have received an intracerebroventricular

43 injection of Aβ oligomers (6). Since synapse loss is considered to adversely affect cognition,

44 reversal or prevention thereof may represent a therapeutic strategy for neurodegenerative

45 diseases (7).

46 Discovery of novel compounds that modulate synapse density most often initiates with *in vitro*

47 screens. In its simplest form, screening is done on primary neuronal cultures, stained for a

48 specific synapse marker (8-10). Among the applications, this approach has been used to

49 document the synaptotoxic effect of $A\beta_{1-42}$, and its prevention by an oligomerization inhibitor

50 (10). However, using a single marker to identify synapses is complicated by the presence of

51 non-synaptic (*e.g.,* vesicular) or degenerate synaptic structures. To focus more specifically on

52 mature synapses, the colocalization between a pre- and postsynaptic marker has been

53 introduced as readout (11-16). Several gene silencing screens have made use of this approach

54 to identify regulators of excitatory and inhibitory synapses (12, 15). Yet, also this approach is

55 not free from caveats, as the use of antibodies limits the sensitivity of the assay to their

56 specificity. While elegant genetic strategies for synapse labeling have been conceived (17),

57 from a screening perspective, immunostaining is preferred for its ease-of-use, universal

58 applicability and lack of overexpression artefacts. One way to validate antibody specificity

59 consists of knocking down the target gene (13, 15). However, such an approach is expensive

60 and may not provide a sufficiently reliable result as the knockdown could be incomplete, off-

61   target and alter the cellular phenotype (*e.g.,* cytotoxic). Hence, a more systematic validation of

62   antibody performance that does not require experimental interventions would be welcome. To

63   satisfy this need, we introduced a segmentation-independent microscopy image analysis of 28

64   commercially available antibodies raised against pre- and postsynaptic proteins on primary

65   cortical and hippocampal cultures. We also quantified the degree of colocalization between pre-

66   and postsynaptic markers and found significant differences in synapse count between different

67   marker combinations. Finally, to improve the sensitivity and reproducibility of synapse density

68   quantification, we introduced a transsynaptic proximity-ligation assay (PLA). Considering the

69   unique property of PLA to only detect protein interactions at distances below 40 nm (18), we

70   identified bonafide partners at the pre- and postsynaptic side. We show that transsynaptic PLA

71   has the specificity and sensitivity necessary to provide reliable synapse counts for *in vitro*

72   experiments aimed at synaptic modulation.

Materials and Methods

Primary neuronal cell culture

This study was carried out in accordance with the recommendations of the ethical committee for animal experimentation of the University of Antwerp (approved ethical file 2015-54). Hippocampi and cortex were dissected from WT C57Bl6 and PSD95-CreNABLED (19) (purchased from the Jackson laboratories, ref 029242). E18 mouse embryos in HEPES (7 mM)-buffered Hanks Balanced Salt Solution (HBSS-HEPES), followed by trypsin digestion (0.05%; 10 min; 37°C) and mechanical dissociation. After centrifugation (5 min at 200g), the cell pellet was resuspended in Minimal Essential Medium supplemented with 10% heat-inactivated normal horse serum and 30 mM glucose. Cells were plated in Poly-D-Lysin-coated 96-well plates (Greiner µClear), at 30,000 cells/cm² (for immunocytochemistry), or in 6-well plates at 60,000 cells/cm² (for western blot) and kept in a humidified CO_2 incubator (37°C; 5% CO_2). After 4 hours, the medium was replaced with 150 µl B27-supplemented Neurobasal medium (NB-B27), containing Sodium Pyruvate (1 mM), Glutamax (2 mM), glucose (30 mM) and Penicillin-Streptomycin (0.5%). To suppress proliferation of non-neuronal cells, 0.5 µM arabinosylcytosine was added in 25 µl NB-B27 at the third and tenth day *in vitro* (DIV). Cell culture supplies were purchased from ThermoFisher (Waltham, MA, USA).

Western blotting

14 DIV cortical and hippocampal cultures were lysed using ice-cold RIPA buffer supplemented with phosphatase and protease inhibitor (HALT cocktail, ThermoFisher 78445) and 5 mM EDTA. The lysate was centrifuged (10.000g, 20 min, 4 °C) and the protein concentration of the supernatant was determined using a BCA assay (ThermoFisher 23225). Samples were denatured (70% sample, 25% LDS, 5% DTT) for 10 min at 70 °C before being loaded on a 4-12% Bis-tris gel (ThermoFisher NP0322BOX) at 10 µg/lane. A stained ruler was included in

98   the first and last well (ThermoFisher 26616). The gel tank was filled with NuPage MOPS SDS

99   running buffer and NuPage anti-oxidant, and was cooled during electrophoresis (200V, ± 1h).

100   Proteins were transferred to a PVDF membrane using NuPage transfer buffer (30V, 1h). To

101   check the transfer, blots were reversibly stained with a 0.1% Ponceau S solution in 5% acetic

102   acid. Blots were subsequently blocked with 5% ECL blocking solution in Tris-buffered Saline

103   with 0.1% Tween (TBS-T). Blots were cut into 5 pieces so that 2 lanes (hippocampal and

104   cortical) with or without the ruler could be stained in 1 reaction. Primary antibody was applied

105   overnight at 4 °C on a roller, followed by a TBS-T wash (3 x 5 min). Horse Radish Peroxidase-

106   coupled secondary antibodies were incubated for 2h at room temperature (RT), followed by a

107   final TBS-T wash. All antibodies were diluted in blocking buffer and are listed in **Suppl. Table**

108   **1**. After reconstructing the cut blots into their original positions, bioluminescent detection was

109   performed using Immobilon Western HRP substrate (Merck Millipore WBKLS0500, 30 sec)

110   and a Chemidoc Touch imager (Biorad, Temse, Belgium). After completion, the blots were

111   restained for GAPDH as loading control. The global contrast of the individual (cut) blots was

112   adjusted with Fiji image analysis freeware (20).

113

114   *Immunofluorescence staining (IF)*

115   Paraformaldehyde-fixed cultures (2%, 20 min, RT) were permeabilized with 1% Triton X-100

116   in blocking buffer (0.1% bovine serum albumin and 10% normal horse serum in PBS) for 10

117   min, followed by an overnight incubation with the primary antibodies (**Suppl. Table 1**) at 4 °C

118   in blocking buffer. After washing with PBS, secondary antibodies (**Suppl. Table 1**) were added

119   for 2 hours. Finally, 4′,6-diamidino-2-phenylindole (DAPI) was applied to the cultures for 10

120   min at a concentration of 2.5 µg/ml, followed by a PBS wash. Primary antibodies targeting

121   extracellular epitopes were incubated prior to permeabilization to reduce non-specific

122   intracellular background staining. This was followed by a PBS wash and permeabilization to

123   continue with antibodies targeting intracellular epitopes. All presynaptic markers were

124   designated to the 561 nm excitation channel, while postsynaptic markers were labeled for the

125   488 nm channel. Secondary antibodies were kept identical where possible, depending on the

126   species of the primary antibody.

127

128   *Expansion microscopy*

129   The protocol for expansion of the samples was adapted from (21). In brief, immunostained

130   samples were crosslinked for 10 min in 0.25% glutaraldehyde in PBS. Gelation was done in a

131   mixture of 2M NaCl, 2.5% (w/w) acrylamide, 0.15% (w/w) N,N'-methylenebisacrylamide,

132   8.625% (w/w) sodium acrylate in PBS with polymerization initiated with TEMED and APS.

133   Polymerized gels were incubated for 30 min at 37°C in a digestion buffer containing 8 U/ml

134   proteinase K. Cover glasses were removed from the digested gels, which were placed in high

135   volumes (> 30 mL) of distilled water that were exchanged at least 5 times until full expansion

136   of the gels. The lateral expansion factor was determined by measuring the gel dimensions before

137   and after expansion. Finally, the gels were trimmed, nuclei counterstained with Hoechst 33342

138   (1/5000 in water for 30 min at room temperature), positioned in 50 mm diameter glass bottom

139   dishes (WillCo Wells GWSt-5040) and immobilized using 2% agarose.

140

141   *Dendritic spine labeling*

142   To label spines in a sparsely distributed subset of neurons, 14 DIV cultures were incubated with

143   the lipophilic dye CM-DiI (ThermoFisher C7000, 5 µg/ml, 20 min), followed by a PBS wash.

144   The next day, after the dye had spread throughout the plasma membrane, the cultures were

145   gently permeabilized using a glycerol gradient (50% glycerol for 20 min, 80% for 20 min and

146   100% for 50 min) followed by an extensive PBS wash. This permeabilization protocol

147   preserved DiI fluorescence while allowing antibody penetration. A similar, but longer protocol

148   was used for IF, in which the primary antibody was applied overnight at room temperature and

149   the secondary for 4 hours.

150

151   *Synaptic Proximity Ligation Assay (synaptic PLA)*

152   Primary cultures fixed and permeabilised as described for IF were used to perform PLA using

153   a commercial kit (Duolink® PLA starter kit, Sigma-Aldrich) according to manufacturer's

154   instructions. Briefly, cells were incubated with a commercial blocking buffer, and then

155   incubated overnight at 4°C, with primary antibodies diluted in the commercial solution at

156   concentrations described in **Suppl. Table 1**. After PLA probe incubation, ligation and

157   amplification steps, samples were immunostained for MAP2 and Synapsin for triple staining

158   experiments, counterstained with Duolink® Nuclear Stain and mounted with anti-fade buffer

159   (Sigma-Aldrich). Images were taken no more than 2 days after the PLA procedure to ascertain

160   signal preservation.

161

162   *Microscopy*

163   Cultures were imaged with a spinning disk confocal high-content imager (Opera Phenix,

164   PerkinElmer) equipped with a robotic arm for plate loading. A 40X water immersion objective

165   (numerical aperture (NA) 1.1) was used. At 488 nm excitation, the optical resolution of the

166   system is 0.271 μm (and corresponding pixel size 0.149 μm), which is considerably larger than

167   the distance of the synaptic cleft (15–25 nm), yet sufficiently small to allow signals of

168   corresponding pre- and postsynaptic markers to partially overlap. Per well, 15 fields were

169   acquired in 4 channels (405nm, 488nm, 561nm and 640nm excitation) at 4 axial positions

170   separated by 1 μm spacing. Different fluorescence channels were separated using standard

171   excitation/emission filters and dichroic mirrors. Owing to the large dynamic range of the Opera

172   Phenix system, acquisition settings could be kept identical for all experiments. For assessing

173   localization of postsynaptic markers in dendritic spines and synaptic PLA triple stainings

174   (synaptic PLA/mVenus/synapsin), a spinning disk confocal research microscope (UltraVIEW

175   VoX, PerkinElmer) was used, equipped with a 60X water objective (NA 1.2) resulting in an

176   optical resolution of ~200 nm and corresponding pixel size of 120 nm. Finally, for super-

177   resolution radial fluctuations (SRRF) microscopy (22), the same setup was used to acquire

178   stacks of 200 images of the same confocal plane, using the Perfect Focus System to prevent

179   focus drift.

180

181   *Image analysis*

182   To assess the degree of colocalization between two synaptic markers, we adopted the *van*

183   *Steensel* approach (23). This method calculates the Pearson correlation coefficient (PCC)

184   between two images as a function of a lateral shift (Δx), resulting in a correlation function (CF).

185   When the image is compared to its (shifted) duplicate, the result is an auto-correlation function

186   (ACF). In case of complete colocalization, the correlation function (CF) has a maximum (PCC

187   = 1) at $\Delta x = 0$ (no shift); in case of exclusion, it reaches a minimum at this position. The shape

188   of the CF not only informs on the presence or absence of colocalization, when colocalization is

189   present, it also provides information on the size of the overlapping spots (the width of the CF

190   measured as full width at half maximum (FWHM)) and the dynamic range – and thus quality –

191   of the staining (measured as the amplitude of the CF). Exactly because of this latter property,

192   the approach was also used to assess the specificity of single synapse marker staining, the

193   assumption being that the ACF of an image decreases with Δx much stronger for a specific

194   staining than it does for less specific ones. The maximal pixel shift used for both analyses was

195   50 pixels in both directions, which is well beyond the typical spot diameter of ~ 10 pixels. The

196   variation across images, or the spread, was expressed by a band of 1 standard deviation above

197   and below the average CCF and measured at dx = 50 px for plotting. All measurements were

198   performed in FIJI image processing freeware using a home-written script that is available upon

199   request.

200   For spot and synapse density quantification, multidimensional images were analyzed using a

201   previously developed image analysis pipeline for Acapella software (PerkinElmer) (16). In

202   brief, nuclei (DAPI) and neurites (MAP2) were segmented based on a user-defined fixed

203   threshold. Non-neuronal nuclei were removed based on their larger size, lower circularity and

204   limited overlap with the neurite mask. Next, both the neurite and neuronal nuclei mask were

205   dilated and subtracted from each other to obtain a search region for synapse marker spots. Spots

206   were enhanced using a Difference of Gaussian filter with a ratio of 1.6. To set thresholds in an

207   unbiased manner, a Fiji script was written that allowed user-friendly interaction with the images

208   while being blinded for the synapse marker at hand. Spot counts were normalized to the neurite

209   area to obtain the spot density. For double stainings and PSD-mVenus experiments, the density

210   of colocalizing spots in 2 fluorescence channels was calculated as those spots for which at least

211   1 pixel overlaps. We previously determined that measurements were not biased by chromatic

212   aberration or the overlap criterion (16). For colocalization of antibodies with PSD95-mVenus,

213   the percentage of PSD95-mVenus spots that have an overlapping synapse marker spot was

214   measured. For double immunostainings, the percentage of all spots that reside in synapses was

215   calculated as the density of colocalizing spots divided by the density of all (colocalizing and

216   non-colocalizing) spots multiplied by 100.

217   For double labeling with dendritic spines, the puncta within a CM-DiI-positive stretch were

218   counted manually on anonymized images and assigned to either the dendritic shaft or spine.

219   The percentage of spots residing in dendritic spines, and the percentage of spines containing

220   spots were calculated. For quantitative distance analysis in synaptic PLA images, center

221   coordinates were extracted for all spots, and the pairwise distance distribution between spot

222   types (PLA, mVenus, Synapsin) was analyzed in R using the package "spatstat" by applying

223   the nearest neighbor correlation (nncorr) method after correcting for the search region (i.e., the

224   neurite mask) (24). For SRRF, the NanoJ plugin for FIJI was used (22). Briefly, after drift

225   correction with NanoCore, a temporal radial auto-correlation of order 2 was applied, with

226   gradient smoothing, intensity weighting and gradient weighting (PSF FWHM = 3.17) for spot

227   channels, and the previous settings with renormalization for the MAP2/DAPI channel.

228

229   *Data visualization and statistics*

230   Graphs were constructed in Graphpad Prism and statistics performed in SAS JMP. For single,

231   double and ENABLED stainings, 6 wells were considered per condition (marker or marker

232   combination and cell type). Within each well, 15 fields were imaged. For statistical comparison

233   of spot densities, these fields were averaged so that 1 data point represented 1 well. A one-way

234   ANOVA was performed using marker as fixed factor followed by post-hoc testing for

235   predefined comparisons (antibodies that had the same target; 7 comparisons) with Sidak's

236   correction. For triple stainings and hTau-P301L overexpression experiments, two-way

237   ANOVA was performed, with marker and PLA type or MOI and method (PLA or

238   colocalization) as fixed factors, respectively. Van Steensel analyses were performed on

239   individual fields, amounting to 90 data points per condition, while segmentation results were

240   averaged per well before plotting (6 data points per condition). For dendritic spine analysis, at

241   least 200 spines were counted per condition. For synaptic PLA experiments a minimum of 4

242   wells with 15 fields per well were averaged per condition. For SRRF of synaptic PLA staining,

243   between of 4 and 7 images were used per combination.

244

245

Results

Not all synapse markers can be labeled with equal specificity

Synapses harbor a unique proteome for which a wealth of dedicated antibodies has been developed. Yet, despite their ample use, the specificity and generalizability of many remains questionable. Therefore, we screened a panel of synapse-targeting antibodies for their labeling specificity on hippocampal and cortical cultures at 14 days *in vitro* (DIV), a time point at which synaptic connections are well-established (16, 25-27). Targets included proteins of pre- (vesicular, active zone) and postsynaptic (receptor, scaffold) compartments, as well as trans-synaptic adhesion proteins (**Suppl. Table 1, Fig. 1a, b**). When quantifying the absolute spot density using a user-defined threshold, we found variable results in that antibodies targeting the same antigen yielded significantly different spot densities (Neurexin, Neuroligin1, GluN1) or a very large variability between replicates (PSD95 (a), Shank) (**Fig. 1a** for cortical and **Suppl. Fig. 1** for hippocampal cultures). Exemplary, the sum of excitatory (vGLUT) and inhibitory (vGAT) spots was not equal to the number of spots stained by a pan-presynaptic marker (Synapsin, Synaptophysin, Bassoon). This suggests that not all antibodies stain with equal specificity and that spurious signals may represent a serious confounding factor.

To rule out bias arising from user-dependent thresholding, we adopted a method for unbiased analysis of IF staining performance, by determining the auto-correlation function (ACF) using the van Steensel approach (23) (see M&M; **Fig. 1c**). The amplitude of the ACF was used as proxy for labeling specificity, the full width at half max (FWHM) reported on the average spot size, whereas the spread (2 x standard deviation at dx = 50 px) around the average ACF informed on the variability between replicates. Based on the dimensions and quality of representative markers, we determined a window in which antibodies were considered to yield an optimal staining result (ACF amplitude > 0.75, FWHM < 11 (= expected spot size) and spread <0.08). All synaptic vesicle and active zone markers met these criteria (**Fig. 1d** for

271   cortical and **Suppl. Fig. 1b** for hippocampal cultures, see **Suppl. Fig. 2** for the actual ACF

272   plots). Except for Neuroligin1 (c), GluA1-4, Homer and PSD95 (a,b), antibodies that target

273   adhesion molecules, neurotransmitter receptors and scaffold proteins yielded more blunted

274   (amplitude < 0.75; FWHM > 11) and variable (spread > 0.08) ACFs, indicative of lower

275   labeling specificity (**Fig. 1d**). Antibodies that target GluA2 and SAP102 yielded exceptionally

276   high FWHM since they also labeled nuclei. For some inhibitory markers (Gephyrin and

277   Neuroligin2), we observed considerable differences in the ACF of hippocampal and cortical

278   cultures, which could point to variations in antigen abundance and inhibitory contacts between

279   the two cell culture types (**Fig. 1d, Suppl. Fig. 1b**).

280   To gain more insight into the specificity of the same synapse antibodies, we performed western

281   blots on cell extracts of 14 DIV cortical and hippocampal cultures (**Suppl. Fig. 3**). Only a

282   minority (4/27; Neurexin (a), Neuroligin1 (a and b), and Shank) of the immunoblot-compatible

283   antibodies failed to label a specific band near the predicted molecular weight of the targeted

284   marker. Neurexin (a) antibody also had a suboptimal ACF, underlining its complete lack of

285   specificity. However, the ACF of Neuroligin1 (a) and (b) and Shank did not show major

286   deviations, suggesting that epitopes may have been lost upon denaturation for western blots.

287   For several markers, multiple bands were commonly detected. These observations need not

288   necessarily imply non-specificity as it may be the result of the extraction/denaturation

289   procedure (exposing masked epitopes) or the presence of alternative isoforms. However,

290   recognition of different isoforms may contribute to variable staining specificity. Notable

291   examples include a Synapsin1/2 antibody which revealed many more isoforms in hippocampal

292   than in cortical culture, and a vGAT antibody, which not only binds the full-length (synaptic)

293   protein, but also a truncated, extra-synaptic variant (28). We conclude from these experiments

294   that immunoblotting does not contribute significantly to the understanding of how antibodies

295   will perform in immunofluorescence, as opposed to unbiased ACF analysis.

296 *Genetic and spine labeling strategies reveal partial synaptic localization*

297 While IF showed that most antibodies yield a punctate staining, it was not clear whether the

298 obtained signals solely represent synapses. That is why we sought for a strategy that could

299 provide more certainty and serve as benchmark for determining synaptic localization. As a first

300 approach, we made use of PSD95-mVenus (ENABLED) transgenic mouse cultures (19). In this

301 model, endogenous PSD95 should be labeled with minimal overexpression artefacts. As we

302 noticed the PSD95-mVenus signal increased with culture age (**Suppl. Fig. 4**), we analyzed the

303 colocalization at both 14 and 28 DIV (**Fig. 2b, Suppl. Fig. 5-7**), using the van Steensel

304 approach. In this case the CCF amplitude reports on the degree of colocalization and the FWHM

305 on the combined size of the spots, as evidenced by simulations (**Fig. 2a**). We also measured the

306 percentage of PSD95-mVenus spots that have an overlapping synapse marker spot using a

307 segmentation-based approach (defined as overlap coefficient; OC). To determine the maximum

308 level of colocalization attainable with both approaches (CCF and segmentation-based), an anti-

309 GFP antibody (which cross-reacts with mVenus) was included as positive control. This control

310 yielded a CCF amplitude of ~ 0.7 and FWHM ~ 10, and upon segmentation, an OC of ~ 80%

311 in cortical cultures at both DIVs (**Fig. 2b,** see **Suppl. Fig. 5** for hippocampal). Given that

312 PSD95-mVenus is an excitatory marker, the amplitude of the CCF and OC were significantly

313 larger for excitatory (*e.g.,* Homer) than for inhibitory (*e.g.,* vGAT, GABA-R) markers at both

314 DIV. Surprisingly, IF with two validated PSD95 (a,b) antibodies – considered positive control

315 as well – only resulted in modest colocalization with the PSD95-mVenus spots. Also, the

316 synaptic adhesion proteins Neurexin (b), Neuroligin1 (c) and Neuroligin2 showed low

317 colocalization with PSD95-mVenus. Of the tested presynaptic markers, Bassoon yielded the

318 highest colocalization with PSD95-mVenus, consistent with its presence in the active zone,

319 whereas vesicle markers (Synapsin, Synaptophysin (a), vGLUT) were further away from the

320 PSD95-mVenus spots (resulting in higher FWHM) and therefore showed lower colocalization

321 (lower amplitude and OC). This benchmarking indicated that the Homer antibody is best suited

322 to label the excitatory postsynaptic compartment and that Bassoon is the preferred presynaptic

323 marker.

324 In a second attempt to validate synaptic localization, we specifically focused on the excitatory

325 postsynaptic compartment. This part of the synapse has a unique structure that is referred to as

326 a dendritic spine (29). Despite significant morphological plasticity, spines can be readily

327 visualized, among others using lipophilic dyes such as DiI (30, 31). When combining DiI with

328 postsynaptic antibody staining, we found considerable differences in colocalization between

329 synapse markers in cultures of 14 DIV (**Fig. 2c**). At the lower limit of the dynamic range,

330 GABA-R puncta were rarely located on spines (6±4% for cortical and 12±9% for hippocampal),

331 which corresponds to findings on cortical tissue at the ultrastructural level (32, 33). To gauge

332 the upper limit of the dynamic range, we considered the genetic PSD95-mVenus signal and

333 found that nearly 80% of the spots were located on spines, and that 80% of all spines contained

334 mVenus signal. AMPA-R clusters, as labeled with GluA1-4 antibody, were partially located on

335 dendritic spines, yet the majority of spots were found on the shaft. For PSD95 (a, b) antibodies,

336 of which we theoretically expected spine labeling similar to PSD95-mVenus (~80%),

337 colocalization was less than half (30-40%) of the anticipated result. This implies that the

338 antibodies did not label their target antigens with sufficient selectivity, as also suggested by the

339 PSD95-mVenus colocalization measurements (**Fig. 3b**). With ~50% of spines being labeled

340 and ~60% of all spots residing on spines, the scaffold protein Homer approached the upper limit

341 of the dynamic range, proving more specific than both PSD95 antibodies.

342 Taken together, there is a substantial fraction of the IF signal that does not align with synapses,

343 and, not all synapses are efficiently labeled by antibodies. Of those antibodies tested, Homer

344 showed the highest colocalization with the PSD95-mVenus signal and strongest enrichment in

345 dendritic spines, indicating that this antibody is best suited to stain the majority of the

346 postsynaptic compartments.

347

348 *Synapse marker colocalization improves selectivity for mature synapses*

349 The previous experiments revealed that synaptic antibodies label synapses with variable

350 specificity and that non-synaptic spots are present, which complicates robust synapse

351 quantification. Yet, using expansion microscopy, we confirmed that pre- and postsynaptic

352 markers are often found juxtaposed in cultures at 14 DIV (**Fig. 3a**). The diffraction limit

353 inherent to conventional fluorescence microscopy precludes signals closer than 200 nm from

354 being resolved. With 20 nm, the synaptic cleft is well below this limit. Thence, a simple

355 approach to detect mature synapses – *i.e.,* synapses that dispose of a clear pre- and postsynaptic

356 compartment – with more certainty consists of quantifying the apparent overlap between pre-

357 and postsynaptic markers (12, 13, 15, 16). We applied this method to synaptic marker antibodies

358 that showed a crisp punctuate staining (evidenced by the ACF criteria defined above) and were

359 raised in different species so that they could be combined in double stainings (**Fig. 3** for cortical,

360 **Suppl. Fig. 8** for hippocampal cultures). Threshold-dependent spot quantification revealed that

361 only a fraction of the pre- and postsynaptic spots resided in mature synapses, as evidenced by

362 the lower density of colocalizing spots compared to the spot density of the individual markers

363 (**Fig. 3b**, **Suppl. Fig. 8a**). The CCF between the two synapse marker channels was calculated,

364 as well as the percentage of spots that reside in synapses (defined as the overlap coefficient,

365 OC; **Fig. 3c**). The large FWHM (> 24 px), small amplitude (< 0.2) of the CFF and a low OC (<

366 5%) for combinations of inhibitory presynaptic and excitatory postsynaptic markers (vGAT and

367 PSD95 (a/b)), or an excitatory presynaptic and inhibitory postsynaptic marker (vGLUT and

368 GABA-R) illustrate that false positive detection by sheer chance is low (**Fig. 3c**, **Suppl. Fig.**

369 **8b**). As positive control, we used a combination of two rabbit polyclonal primary antibodies

370   (vGAT and Homer), onto which the secondary antibodies were expected to bind with equal

371   affinity. The resulting CCF had a large amplitude (> 0.65) and small FWHM (< 15 px; **Fig. 3c**,

372   **Suppl. Fig. 8b**), while the CCF approached a value of 1 at $\Delta x=0$ (**Suppl. Fig. 9-10**), consistent

373   with perfect colocalization. The OC on the other hand, amounted to only 56% for cortical and

374   44% for hippocampal cultures, again showing the strength of the unbiased CCF approach over

375   spot segmentation. The colocalization (CCF and OC) was reduced when using two markers that

376   label the same compartment (Synaptophysin (a)/Bassoon and Synapsin/Bassoon). Despite this

377   limitation to the dynamic range, clear patterns could still be discriminated. For example, the

378   combination of a pan-presynaptic marker (Synapsin or Synaptophysin (a)) with an inhibitory

379   marker (GABA-R) could be distinguished from the combination with excitatory markers

380   (PSD95 (a/b), Homer) (**Fig. 3c, Suppl. Fig. 8b**). The smaller FWHM, higher amplitude and

381   larger OC indicate that the excitatory markers were closer to the presynaptic markers. Our

382   results also indicated that GluA1-4 shows low colocalization with pan-(Synapsin,

383   Synaptophysin) and excitatory (vGLUT) presynaptic markers, suggesting that many AMPA-R

384   clusters reside outside of the synapse. In cortical as well as hippocampal cultures, Bassoon-

385   Homer proved to be the combination with the highest colocalization, confirming that this

386   combination is preferred for detecting mature synapses.

387

388   *Proximity of markers allows selective labeling of mature synapses*

389   As the colocalization of two markers might be confounded by the presence of spurious signals

390   (*e.g.,* extrasynaptic staining), we sought for an approach that would only give rise to positive

391   signals in case pre- and postsynaptic markers are sufficiently close. We reasoned that the

392   Proximity Ligation Assay (PLA) (34) would represent a plausible method to achieve this, as it

393   only leads to a reaction when two markers (and their respective antibodies) are closer than 40

394   nm, a distance range that bridges the synaptic cleft (35) (**Fig. 4a**). We first validated the concept

395   using a positive control – antibodies for lamin A and lamin B1, two nuclear envelope markers

396   that are known to interact directly (36) – and a negative control – antibodies targeting lamin A

397   and the mitochondrial marker TOMM20, which are spatially separated by much more than 40

398   nm. The positive control yielded nuclear-localized PLA spots, whereas the negative control

399   produced virtually no signal, as was the case for a negative technical control in which only one

400   of the primary antibodies was used (**Suppl. Fig. 11a**). Next, we tested whether targeting pairs

401   of proteins present in excitatory and inhibitory synapses resulted in a synaptic PLA reaction.

402   We found that the negative control - targeting vGLUT (excitatory) and Neuroligin 2 (inhibitory)

403   – yielded a low PLA signal, whereas PLA for vGLUT and Neuroligin 1 (c) (both excitatory

404   synapse markers) produced a strong punctate PLA pattern along the neurites, consistent with a

405   synaptic staining. The synaptic PLA spot density fell within the range of values found for dual

406   immunofluorescence against Homer/Bassoon (~0.05 spots/μm^2). We noted that the amount of

407   synaptic PLA signal with the combination VGAT-Neuroligin1 (a discordant excitatory-

408   inhibitory combination) was higher than for VGAT/Neuroligin2 which should detect reaction

409   on inhibitory synapses only (**Suppl. Fig. 11b**).

410   To maximize the efficiency of the PLA reaction, we selected within our panel of antibodies,

411   those that would bind markers that directly interact. We selected Neurexin 1 (b) as the most

412   suitable pan-synaptic marker since it has been proven that it interacts at the molecular level

413   with the extracellular epitopes of 4 postsynaptic proteins with available antibodies, namely:

414   anti-GluA1-4, anti-GABA-R, anti-Neuroligin1 (c), and anti-Neuroligin2 (37-39). Indeed, all 4

415   combinations yielded characteristic punctate PLA pattern at the expected location: inhibitory

416   synapse markers (GABA-R and Neuroligin2) preferentially located near neuronal somas,

417   whereas excitatory PLA signals (GluA1-4 and Neuroligin1 (c)) were found evenly distributed

418   along the neurites (**Fig. 4a**). ACF plots from synaptic PLA displayed a large range (between

419   0.82 and 0.93) and small FWHM (ranging between 7.5 to 10.5px) which would set the quality

420   of the staining as one of the best performing compared to single staining antibodies (**Suppl.**

421   **Fig. 11c**) and outperforming all combinations for double staining.

422

423   *Synaptic counterstaining and superresolution reveals synaptic PLA signal offset*

424   We next investigated the subcellular location of synaptic PLA signal for the most optimal PLA

425   pairs Neurexin/Neuroligin1 and Neurexin/Neuroligin2. To this end, we used ENABLED

426   neuronal cultures at 28 DIV and counterstained for the pan-synaptic marker Synapsin (**Fig. 4c**).

427   Synaptic PLA density measurements were significantly higher for Neurexin/Neuroligin1 than

428   Neurexin/Neuroligin2 (0.18 ± 0.02 vs 0.12 ± 0.01 spots/μm^2; two-way ANOVA, post-hoc

429   Sidak's test p-value = 0.036). Importantly, the densities of synaptic PLA spots, and synaptic

430   PLA/synapsin, synaptic PLA/mVenus pairs are within the ranges obtained previously by double

431   immunofluorescence colocalisation ($0.05 - 0.2$ spots/μm^2) (**Suppl. Fig. 12d**). As mVenus signal

432   is coupled to PSD95, resident in excitatory synapses, we focused on spots densities and overlap

433   of the synaptic PLA for the excitatory combination Neurexin/Neuroligin1. The OC of synaptic

434   PLA signals with mVenus and synapsin was $46\%\pm6$ and $39\%\pm2$, respectively, indicating that

435   less than half of the PLA signals colocalized with one of these markers. This was lower than

436   the OC between mVenus and synapsin ($61\% \pm 6$) (**Suppl. Fig. 12a**). However, when putting

437   the images under scrutiny, we noticed that many of the PLA signals were juxtaposed to the

438   other signals (**Fig. 4b**). To corroborate this, we performed a nearest neighbor correlation

439   analysis between the distributions of detected objects of each marker pair (PLA/mVenus,

440   PLA/synapsin, mVenus/synapsin). In brief, we calculated the probability that the nearest

441   neighbor of a given spot is of a different marker type versus the probability that it could be

442   either of both markers (random distribution). Thus, if both markers were completely

443   independent, the resulting nearest neighbor ratio value (nncorr) would be 1, whereas a

444   completely correlated set would have a ratio value close to 0 (Schematic at **Supl. Fig. 12b**). We

445   found that the nncorr measures for synaptic PLA combinations ranged between 0.05 ± 0.001

446   and 0.19 ± 0.03, suggesting strong dependence with the other markers, as also confirmed by

447   positive (Homer-Bassoon) and negative (vGAT – PSD95) controls (**Suppl. Fig. 12b**).

448   To obtain a more resolved view on the actual distances between the PLA signals and the other

449   markers, we employed SRRF (**Fig. 4c**). We found that 95% of the synaptic PLA signals were

450   closer than 230 nm to Synapsin spots (**Fig. 4c, Suppl. Fig 13a**). The average number of

451   Synapsin spots associated with every synaptic PLA spot was 0.95 ± 0.1, which suggests that

452   synaptic PLA spots are in a 1:1 ratio with synapses. When quantifying the spot density in SRRF

453   images, we found that the density of mVenus and Synapsin spots was 0.45 ± 0.13 and $1.08 \pm$

454   0.2 spots/μm^2 respectively, whereas that of synaptic PLA (or PLA with other marker

455   combinations) was ≤ 0.25 spots/μm^2, similar to IF measurements (**Suppl. Fig. 13b**). Taking

456   advantage of the increased resolution in SRRF images, we measured the average distance

457   between the nearest neighbors from pairs of all marker types. This confirmed that PLA spots

458   were always found in closer proximity to mVenus (0.49 μm) or Synapsin ($0.54 \mu m$) spots than

459   to other PLA spots (**Fig. 4c**). Despite our restriction to optical sections of 0.4 μm, triplets of

460   synaptic PLA, mVenus and Synapsin were frequently encountered with a density of 0.13 spots/

461   μm^2 and constituting $46\% \pm 12$ of total synaptic PLA particles (**Suppl. Fig. 13a**). Thus, the

462   density of synaptic PLA spots aligns well with that of best-performing transsynaptic marker

463   combinations, although they occupy a spatial location that is slightly offset from the actual

464   synapses.

465

466   *Synaptic PLA increases sensitivity for detecting synapse density changes*

467   As we have previously shown synapse density to scale with culture time (Verschuuren et al.,

468   2019), we decided to further validate synaptic PLA on a set of cultures of increasing maturity

469   (DIV 7, 14, 21). As expected, we found an increase in synapse density (**Fig. 5a**). However, the

470   increase between DIV 7 and DIV 21 as measured by synaptic PLA was ~2 fold higher than the

471   best co-localization approach (Bassoon/Homer). We next tested whether synaptic PLA could

472   also pick up changes in synapse density as evoked by pathological conditions. We previously

473   found that overexpression of hTau-P301L reduces synapse density from DIV 14 onwards (16).

474   To assess the sensitivity of this assay, we measured synaptic density at 21 DIV after applying

475   increasing multiplicities of infection (300, 400 and 500 MOI) of the hTau-P301L construct. We

476   found a statistically significant decrease of synaptic PLA spot density in hTau-P301L neurons

477   as compared to control cultures (from 0.20 to 0.18, 0.17 and 0.12 spots/μm^2 for 300, 400 and

478   500 MOI respectively), which was much more prominent than that of the original colocalization

479   approach (Bassoon-Homer), which only yielded a significant decrease starting for MOI400

480   (**Fig. 5b**). In light of this, we next assessed whether the synaptic PLA reaction could

481   differentiate between groups where the colocalization approach was not yet sensitive enough.

482   When testing the lowest hTau-P301L construct concentration (300MOI) at an earlier timepoint

483   (DIV14), a statistically significant difference in synaptic density could be detected with

484   synaptic PLA (two-way ANOVA main effect of PLA vs IF (1,36) = 15.52, p = .003, Sidak's

485   post-hoc test synaptic PLA CTR vs P3011 p<0.001) (**Fig. 5b**). Thus, these results suggest that

486   synaptic PLA allows detecting changes in synapse density more sensitively than the

487   colocalization approach.

488

Discussion

489

490   A wealth of studies has used immunofluorescence to quantify synapse density changes in

491   primary neuronal cultures (6, 8-16, 31, 40). Yet, very few have truly documented the specificity

492   of the utilized antibodies in detail. To gain more certainty about labeling performance, and

493   provide a reference for the field, we have now explored a variety of benchmarking methods to

494   evaluate the specificity of a set of antibodies raised against synaptic proteins. Although

495   extensively used (42), we found that western blotting is not useful for routine antibody

496   validation since neither the presence of additional bands (alternative splice forms) nor the

497   absence of a specific band (epitope masking) can truly predict non-specificity. Therefore, we

498   first introduced a segmentation-independent method to assess the staining performance of

499   individual antibodies in immunofluorescence images. This revealed a large variability between

500   antibodies, which partially depended on the functional class. Synaptic vesicle markers yielded

501   consistently better results in ACF analysis than neurotransmitter receptors or adhesion proteins,

502   likely because the local protein abundance is higher for the former. We further found that the

503   absolute spot density was highly variable even for antibodies that target the same marker. This

504   may be caused by non-specific labeling, low SBR complicating thresholding, and the presence

505   of spurious signals such as markers being trafficked in the neurites or extrasynaptic

506   neurotransmitter receptors. These caveats do not necessarily preclude relative quantification in

507   a setting where experimental conditions are compared to an internal control (8-10), but they

508   may significantly affect sensitivity and render the assay susceptible to confounding factors such

509   as neurotoxicity. By quantifying the association with the postsynaptic compartment, we

510   discovered that Homer outperformed both PSD95 antibodies, both in terms of overlap with the

511   genetic marker PSD95-mVenus and with the presence in dendritic spines. Surprisingly, and in

512   contrast with other reports, we could not recapitulate equally good results with PSD95

513   antibodies (43). This may be due to the different species (rat vs mouse primary hippocampal

514   cultures) or cultivation protocol (Lagache et al. used astrocyte-conditioned medium). Another

515   explanation may be that Homer, as polyclonal antibody, might be more resistant to epitope

516   masking than PSD95 monoclonals. As exponent, the GluA1-4 antibody showed remarkable low

517   correlation with the postsynaptic compartment, suggesting that many AMPA-R clusters reside

518   outside of the synapse, potentially in reserve pools awaiting synaptic potentiation (44).

519   We further found that the selectivity for mature synapses could be enhanced by considering the

520   apparent colocalization between a pre- and postsynaptic marker, while maintaining high-

521   content screening compatibility. The positive results from ACF and downstream analyses for

522   Bassoon and Homer antibodies were further substantiated by the high colocalization metrics

523   (CCF amplitude > 0.45, OC > 30%) when used in combination. This makes the latter

524   combination preferred for global assessment of structural connectivity.

525   While colocalization helps focusing on the relevant fraction of immunolabeled samples, it is

526   subject to bias and suffers from a limited dynamic range. Therefore, we explored whether PLA

527   could serve as a more sensitive alternative. Whereas the PLA technique has been used as a

528   synaptic detection method for tagged proteins, and to localize synaptic proteins to the pre- or

529   post-synaptic compartment (45-47), our work significantly expands the application radius by

530   applying it to transsynaptic connections, rendering it applicable to the detection of mature

531   synapses. Our results demonstrate that synaptic PLA might have additional advantages. First,

532   it allows for much simpler signal detection, as also proven by ACF analysis. Importantly, we

533   found that on average each synaptic PLA spot had ~1 Synapsin spot, which supports the case

534   that synaptic PLA is a reliable proxy for synapse estimates. Second, using one single marker

535   for synaptic connections frees one channel for additional staining. Finally, our results of

536   synapse quantification in cultures through stages of maturation and pathological perturbations,

537   strongly endorse the potential of synaptic PLA being more sensitive and thus capable of

538   detecting subtler changes in synapse number. This is especially relevant for dense cultures, in

539 which crowding may complicate signal detection. On the downside, one has to consider the

540 increased cost and fast degradation of the PLA signal, which, as yet, may limit its applicability

541 in a high-throughput setting. The offset we encountered between PLA signals and antibody

542 labeling, is most likely due to the amplification protocol, but also should be kept in mind.

543 Another potential issue is the detection of PLA signal in controls that were initially considered

544 to be negative (such as VGAT and Neuroligin1). However, it is becoming clearer that the

545 histological definition of inhibitory vs. excitatory synapses is not clear-cut. For example, in

546 cortical culture, electron microscopy of dendritic spines, once thought to be exclusive of

547 excitatory synapses, also contain inhibitory contacts (32). Additionally, Neuroligin1 and

548 Neuroligin2 have been shown to colocalize with both vGAT and vGlut1, with only enrichment

549 of each isoform on excitatory and inhibitory synapses respectively, but by no means an

550 exclusive colocalization (48).

551 To conclude, we have extensively validated synapse antibodies in primary cortical and

552 hippocampal culture and demonstrated that synaptic PLA can be more sensitive than synapse

553 detection by marker colocalization. Our work therefore adds a valuable new angle to synapse-

554 oriented *in vitro* screening assays.

555

References

1. Fein JA, Sokolow S, Miller CA, Vinters HV, Yang F, Cole GM, et al. Co-localization of amyloid beta and tau pathology in Alzheimer's disease synaptosomes. The American Journal of Pathology. 2008;172(6):1683-1692.

2. Pickett EK, Koffie RM, Wegmann S, Henstridge CM, Herrmann AG, Colom-Cadena M, et al. Non-fibrillar oligomeric amyloid-beta within synapses. Journal of Alzheimer's Disease. 2016;53(3):787-800.

3. Scheff SW, Price DA, Schmitt FA, Mufson EJ. Hippocampal synaptic loss in early Alzheimer's disease and mild cognitive impairment. Neurobiology of Aging. 2006;27(10):1372-1384.

4. Koffie RM, Meyer-Luehmann M, Hashimoto T, Adams KW, Mielke ML, Garcia-Alloza M, et al. Oligomeric amyloid β associates with postsynaptic densities and correlates with excitatory synapse loss near senile plaques. Proceedings of the National Academy of Sciences. 2009;106(10):4012-4019.

5. Mucke L, Masliah E, Yu GQ, Mallory M, Rockenstein EM, Tatsuno G, et al. High-level neuronal expression of abeta 1-42 in wild-type human amyloid protein precursor transgenic mice: synaptotoxicity without plaque formation. Journal of Neuroscience. 2000;20(11):4050-4058.

6. Jin M, Selkoe DJ. Systematic analysis of time-dependent neural effects of soluble amyloid β oligomers in culture and in vivo: Prevention by scyllo-inositol. Neurobiology of Disease. 2015;82:152-163.

7. Jackson J, Jambrina E, Li J, Marston H, Menzies F, Phillips K, et al. Targeting the synapse in Alzheimer's disease. Frontiers in Neuroscience. 2019;13(735).

579   8. Nguyen L, Wright S, Lee M, Ren Z, Sauer J-M, Hoffman W, et al. Quantifying amyloid beta

580   (Aβ)–mediated changes in neuronal morphology in primary cultures: implications for

581   phenotypic screening. Journal of Biomolecular Screening. 2012;17(6):835-842.

582   9. Harrill JA, Robinette BL, Mundy WR. Use of high content image analysis to detect chemical-

583   induced changes in synaptogenesis in vitro. Toxicology in Vitro 2011;25(1):368-387.

584   10. Evans NA, Facci L, Owen DE, Soden PE, Burbidge SA, Prinjha RK, et al. Abeta(1-42)

585   reduces synapse number and inhibits neurite outgrowth in primary cortical and hippocampal

586   neurons: a quantitative analysis. Journal of Neuroscience Methods. 2008;175(1):96-103.

587   11. Flavell SW, Cowan CW, Kim TK, Greer PL, Lin Y, Paradis S, et al. Activity-dependent

588   regulation of MEF2 transcription factors suppresses excitatory synapse number. Science.

589   2006;311(5763):1008-1012.

590   12. Nieland TJF, Logan DJ, Saulnier J, Lam D, Johnson C, Root DE, et al. High content image

591   analysis identifies novel regulators of synaptogenesis in a high-throughput RNAi screen of

592   primary neurons. PloS One. 2014;9(3):e91744.

593   13. Paradis S, Harrar DB, Lin Y, Koon AC, Hauser JL, Griffith EC, et al. An RNAi-based

594   approach identifies molecules required for glutamatergic and GABAergic synapse

595   development. Neuron. 2007;53(2):217-232.

596   14. Schatzle P, Wuttke R, Ziegler U, Sonderegger P. Automated quantification of synapses by

597   fluorescence microscopy. Journal of Neuroscience Methods. 2012;204(1):144-149.

598   15. Sharma K, Choi SY, Zhang Y, Nieland TJ, Long S, Li M, et al. High-throughput genetic

599   screen for synaptogenic factors: identification of LRP6 as critical for excitatory synapse

600   development. Cell Reports. 2013;5(5):1330-1341.

601   16. Verschuuren M, Verstraelen P, Garcia-Diaz Barriga G, Cilissen I, Coninx E, Verslegers M,

602   et al. High-throughput microscopy exposes a pharmacological window in which dual leucine

603   zipper kinase inhibition preserves neuronal network connectivity. Acta Neuropathologica

604   Communications. 2019;7(93).

605   17. Lee H, Oh WC, Seong J, Kim J. Advanced fluorescence protein-based synapse-detectors.

606   Frontiers in Synaptic Neuroscience. 2016;8(16).

607   18. Fredriksson S, Gullberg M, Jarvius J, Olsson C, Pietras K, Gustafsdottir SM, et al. Protein

608   detection using proximity-dependent DNA ligation assays. Nature Biotechnology.

609   2002;20(5):473-477.

610   19. Fortin DA, Tillo SE, Yang G, Rah JC, Melander JB, Bai S, et al. Live imaging of

611   endogenous PSD-95 using ENABLED: a conditional strategy to fluorescently label endogenous

612   proteins. Journal of Neuroscience. 2014;34(50):16698-16712.

613   20. Schindelin J, Arganda-Carreras I, Frise E, Kaynig V, Longair M, Pietzsch T, et al. Fiji: an

614   open-source platform for biological-image analysis. Nature Methods. 2012;9(7):676-682.

615   21. Chozinski TJ, Halpern AR, Okawa H, Kim HJ, Tremel GJ, Wong RO, et al. Expansion

616   microscopy with conventional antibodies and fluorescent proteins. Nature Methods.

617   2016;13(6):485-493.

618   22. Culley S, Tosheva KL, Matos Pereira P, Henriques R. SRRF: Universal live-cell super-

619   resolution microscopy. The International Journal of Biochemistry & Cell Biology.

620   2018;101:74-83.

621   23. van Steensel B, van Binnendijk EP, Hornsby CD, van der Voort HT, Krozowski ZS, de

622   Kloet ER, et al. Partial colocalization of glucocorticoid and mineralocorticoid receptors in

623   discrete compartments in nuclei of rat hippocampus neurons. Journal of Cell Science.

624   1996;109(4):787-792.

625   24. Baddeley A, Turner R. Spatstat: An R package for analyzing spatial point patterns. Journal

626   of Statistical Software. 2005;12(6).

627   25. Lesuisse C, Martin LJ. Long-term culture of mouse cortical neurons as a model for neuronal

628   development, aging, and death. Journal of Neurobiology. 2002;51(1):9-23.

629   26. Ichikawa M, Muramoto K, Kobayashi K, Kawahara M, Kuroda Y. Formation and

630   maturation of synapses in primary cultures of rat cerebral cortical cells: an electron microscopic

631   study. Neuroscience Research. 1993;16(2):95-103.

632   27. Grabrucker A, Vaida B, Bockmann J, Boeckers TM. Synaptogenesis of hippocampal

633   neurons in primary cell culture. Cell and Tissue Research. 2009;338(3):333-341.

634   28. Gomes JR, Lobo AC, Melo CV, Inácio AR, Takano J, Iwata N, et al. Cleavage of the

635   vesicular GABA transporter under excitotoxic conditions is followed by accumulation of the

636   truncated transporter in nonsynaptic sites. Journal of Neuroscience. 2011;31(12): 4622-4635.

637   29. Segal M. Dendritic spines: Morphological building blocks of memory. Neurobiology of

638   Learning and Memory. 2017;138:3-9.

639   30. Papa M, Bundman MC, Greenberger V, Segal M. Morphological analysis of dendritic spine

640   development in primary cultures of hippocampal neurons. Journal of Neuroscience.

641   1995;15(1):1-11.

642   31. Verstraelen P, Pintelon I, Nuydens R, Cornelissen F, Meert T, Timmermans JP.

643   Pharmacological characterization of cultivated neuronal networks: relevance to synaptogenesis

644   and synaptic connectivity. Cellular and Molecular Neurobiology. 2014;34(5):757-776.

645   32. Kubota Y, Karube F, Nomura M, Kawaguchi Y. The diversity of cortical inhibitory

646   synapses. Frontiers in Neural Circuits. 2016;10:27.

647   33. Kwon T, Merchán-Pérez A, Rial Verde EM, Rodríguez J-R, DeFelipe J, Yuste R.

648   Ultrastructural, molecular and functional mapping of GABAergic synapses on dendritic spines

649   and shafts of neocortical pyramidal neurons. Cerebral Cortex. 2018;29(7):2771-2781.

650   34. Leuchowius K-J, Clausson C-M, Conze T, Jarvius M, Howell WM, Kamali-Moghaddam

651   M, et al. Proximity ligation assays: a recent addition to the proteomics toolbox. Expert Review

652   of Proteomics. 2010;7(3):401-410.

653   35. Savtchenko LP, Rusakov DA. The optimal height of the synaptic cleft. Proceedings of the

654   National Academy of Sciences. 2007;104(6):1823-1831.

655   36. Kapinos LE, Schumacher J, Mucke N, Machaidze G, Burkhard P, Aebi U, et al.

656   Characterization of the head-to-tail overlap complexes formed by human lamin A, B1 and B2

657   "half-minilamin" dimers. Journal of molecular biology. 2010;396(3):719-731.

658   37. Sudhof TC. Synaptic neurexin complexes: a molecular code for the logic of neural circuits.

659   Cell. 2017;171(4):745-769.

660   38. Zhang C, Atasoy D, Arac D, Yang X, Fucillo MV, Robison AJ, et al. Neurexins physically

661   and functionally interact with GABA(A) receptors. Neuron. 2010;66(3):403-416.

662   39. Mondin M, Labrousse V, Hosy E, Heine M, Tessier B, Levet F, et al. Neurexin-neuroligin

663   adhesions capture surface-diffusing AMPA receptors through PSD-95 scaffolds. Journal of

664   Neuroscience. 2011;31(38):13500-13515.

665   40. Hagmeyer S, Mangus K, Boeckers TM, Grabrucker AM. Effects of trace metal profiles

666   characteristic for autism on synapses in cultured neurons. Neural Plasticity. 2015;16.

667   41. Davey F, Hill M, Falk J, Sans N, Gunn-Moore FJ. Synapse associated protein 102 is a novel

668   binding partner to the cytoplasmic terminus of neurone-glial related cell adhesion molecule.

669   Journal of Neurochemistry. 2005;94(5):1243-1253.

670   42. Signore M, Reeder KA. Antibody validation by Western blotting. Methods in Molecular

671   Biology. 2012;823:139-155.

672   43. Lagache T, Grassart A, Dallongeville S, Faklaris O, Sauvonnet N, Dufour A, et al. Mapping

673   molecular assemblies with fluorescence microscopy and object-based spatial statistics. Nature

674   Communications. 2018;9(1):698.

675 44. Kneussel M, Hausrat TJ. Postsynaptic neurotransmitter receptor reserve pools for synaptic

676 potentiation. Trends in Neurosciences. 2016;39(3):170-182.

677 45. Eagleson KL, Milner TA, Xie Z, Levitt P. Synaptic and extrasynaptic location of the

678 receptor tyrosine kinase met during postnatal development in the mouse neocortex and

679 hippocampus. The Journal of Comparative Neurology. 2013;521(14):3241-3259.

680 46. Almandoz-Gil L, Persson E, Lindstrom V, Ingelsson M, Erlandsson A, Bergstrom J. In situ

681 proximity ligation assay reveals co-localization of alpha-synuclein and SNARE proteins in

682 murine primary neurons. Frontiers in Neurology. 2018;9(180).

683 47. Lundgren JL, Ahmed S, Schedin-Weiss S, Gouras GK, Winblad B, Tjernberg LO, et al.

684 ADAM10 and BACE1 are localized to synaptic vesicles. Journal of Neurochemistry.

685 2015;135(3):606-615.

686 48. Chih B, Gollan L, Scheiffele P. Alternative splicing controls selective trans-synaptic

687 interactions of the neuroligin-neurexin complex. Neuron. 2006;51(2):171-178.

688

Funding

Author contributions

PV, GG, RN, PL and WDV have conceived the work and performed data analysis. PV, GG and BA have performed the wet lab work. MV has developed the synapse quantification script. PV, GG and WDV have drafted the manuscript. All authors have critically revised the manuscript and approved it for publication.

Acknowledgements

702 **Figures**

703
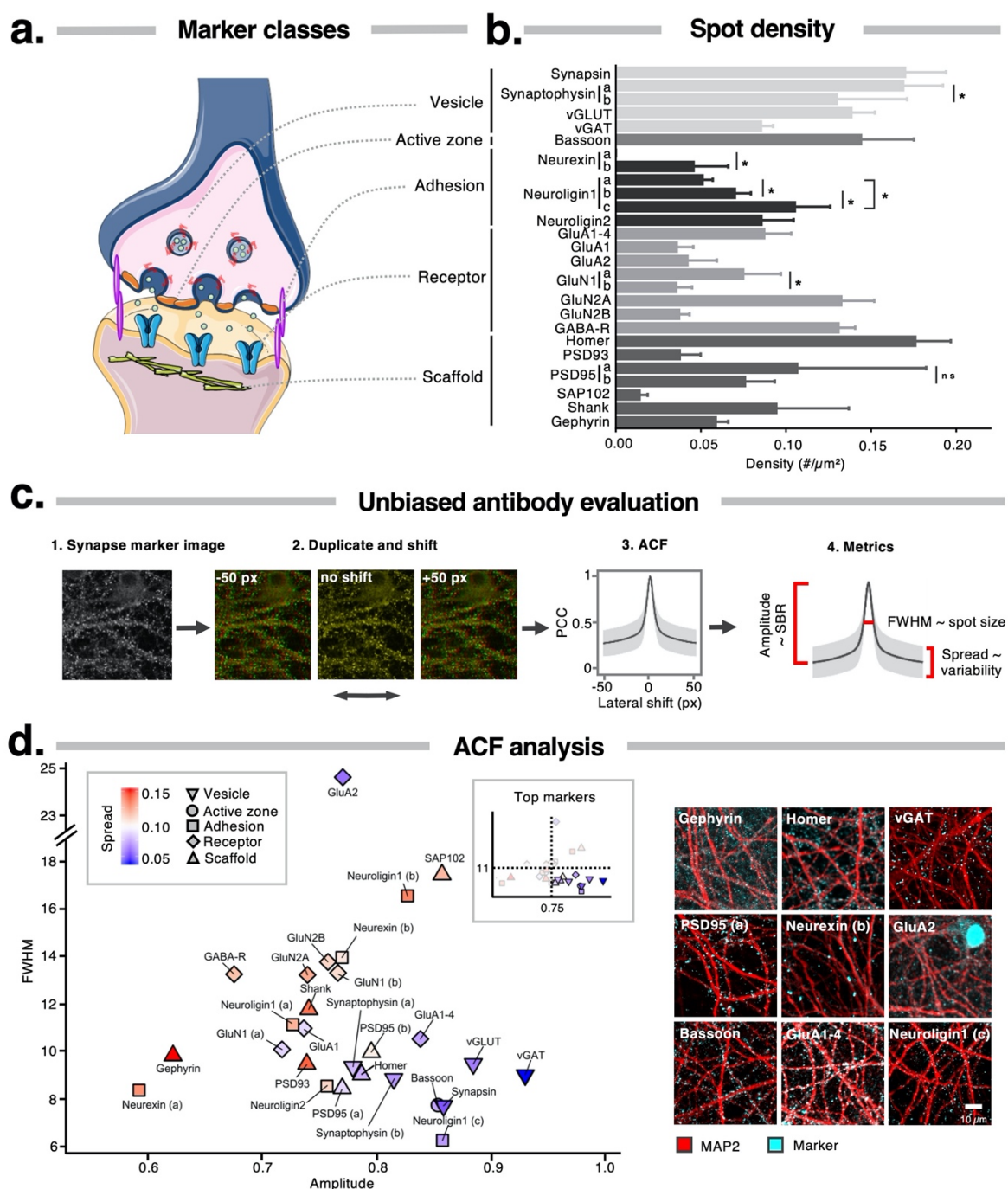
Figure 1. Antibodies targeting synapse markers have variable specificity. **a.** Markers of different functional classes considered in this work; **b.** Quantification of the spot density after immunostaining yields variable results even between antibodies that target the same marker (* $p < 0.05$, one-way ANOVA post-hoc Sidak's multiple comparisons test); **c.** The auto-correlation function (ACF) allows unbiased evaluation of staining performance, by calculating

709   the Pearson's Correlation Coefficient (PCC) between an image and its duplicate as a function

710   of a lateral shift. The ACF amplitude and spread report on the signal-to-background ratio and

711   the variability across images, respectively, the full width at half maximum (FWHM) correlates

712   with spot size. A crisp synapse spot image has a high amplitude (> 0.75) with narrow spread ($<$

713   0.08) and small FWHM (≤ 11), whereas a noisy image has a small amplitude with large standard

714   deviation and large FWHM; **d.** Scatterplot of ACF parameters for the different synapse

715   antibodies tested on primary cortical cultures at 14 DIV, along with representative images for

716   a selected subset. Inset shows the same scatterplot after gating for optimal parameters.
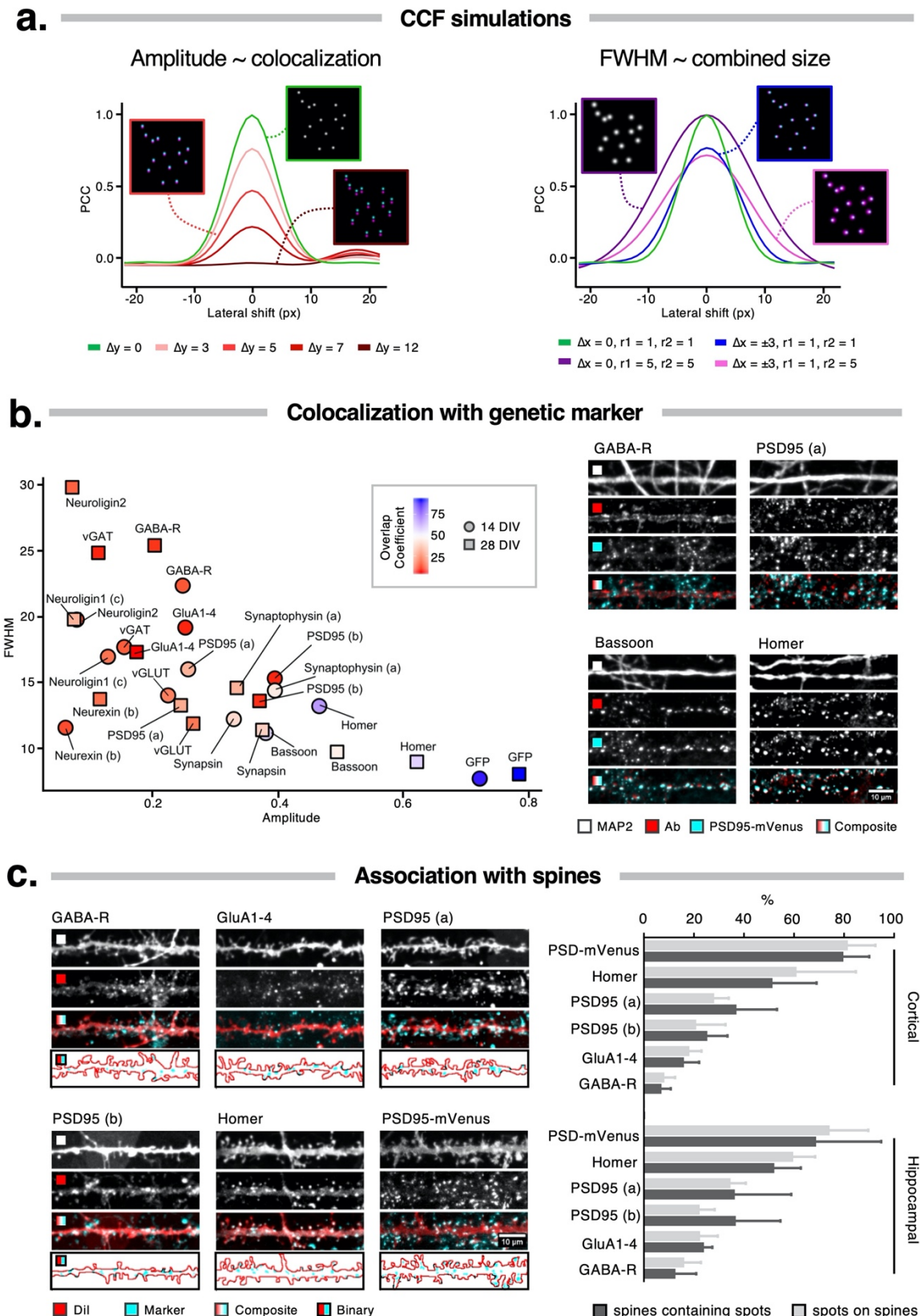
Figure 2. Association of synapse markers with the postsynaptic compartment. **a.** Cross-Correlation Functions (CCFs) for simulated spot images. An increasing mismatch between

720   images (simulated by means of global lateral translation in y by 3, 5, 7 or 12 pixels) results in

721   a progressively lower amplitude, while the FWHM increases with the size of the spots in at

722   least one of both channels and is less sensitive to mismatch (simulated by randomly shifting

723   spots 3 pixels up or down); **b.** Colocalization of synapse marker stainings with the genetic label

724   PSD95-mVenus in 14 and 28 DIV primary cortical cultures, shown in a scatter plot from CCF

725   parameters and color-coded by the overlap coefficient, defined as the percentage of PSD95-

726   mVenus spots that have an overlapping signal from an antibody spot. An anti-GFP antibody,

727   which cross-reacts with mVenus was used as a positive control. Representative images are from

728   28 DIV cortical cultures; **c.** Exemplary dendrite stretches from 14 DIV cortical cultures after

729   co-labeling with postsynaptic synapse markers and DiI. Quantification of the association with

730   spines was done in both cortical and hippocampal cultures.
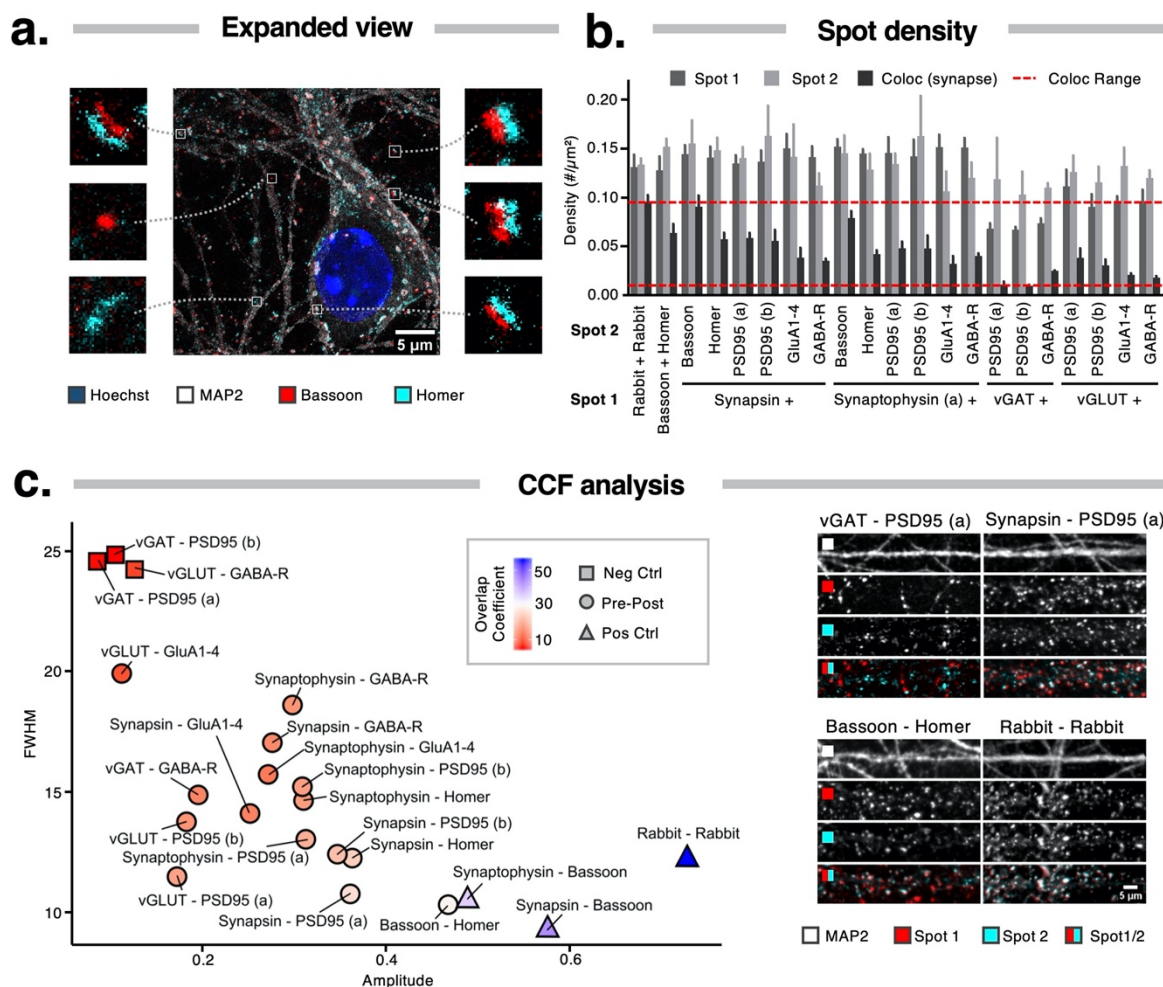
731

732

Figure 3. Quantification of synapse marker colocalization improves selectivity for mature synapses. **a.** Expansion microscopy shows the presence of juxtaposed pre- and postsynaptic signals in 14 DIV cortical cultures, as well as single marker spots; **b.** Quantification of spot and synapse density in 14 DIV cortical cultures shows the fraction of colocalized signals, assumed to represent mature synapses; **c.** Scatter plot of CCF parameters reporting on the colocalization of marker pairs in 14 DIV cortical neurons. The color code indicates the overlap coefficient, defined as the percentage of spots that reside in synapses. Pairs of inhibitory with excitatory synapse markers were considered negative controls while 2 pan-presynaptic markers and primary antibodies raised in the same species were used as positive controls.
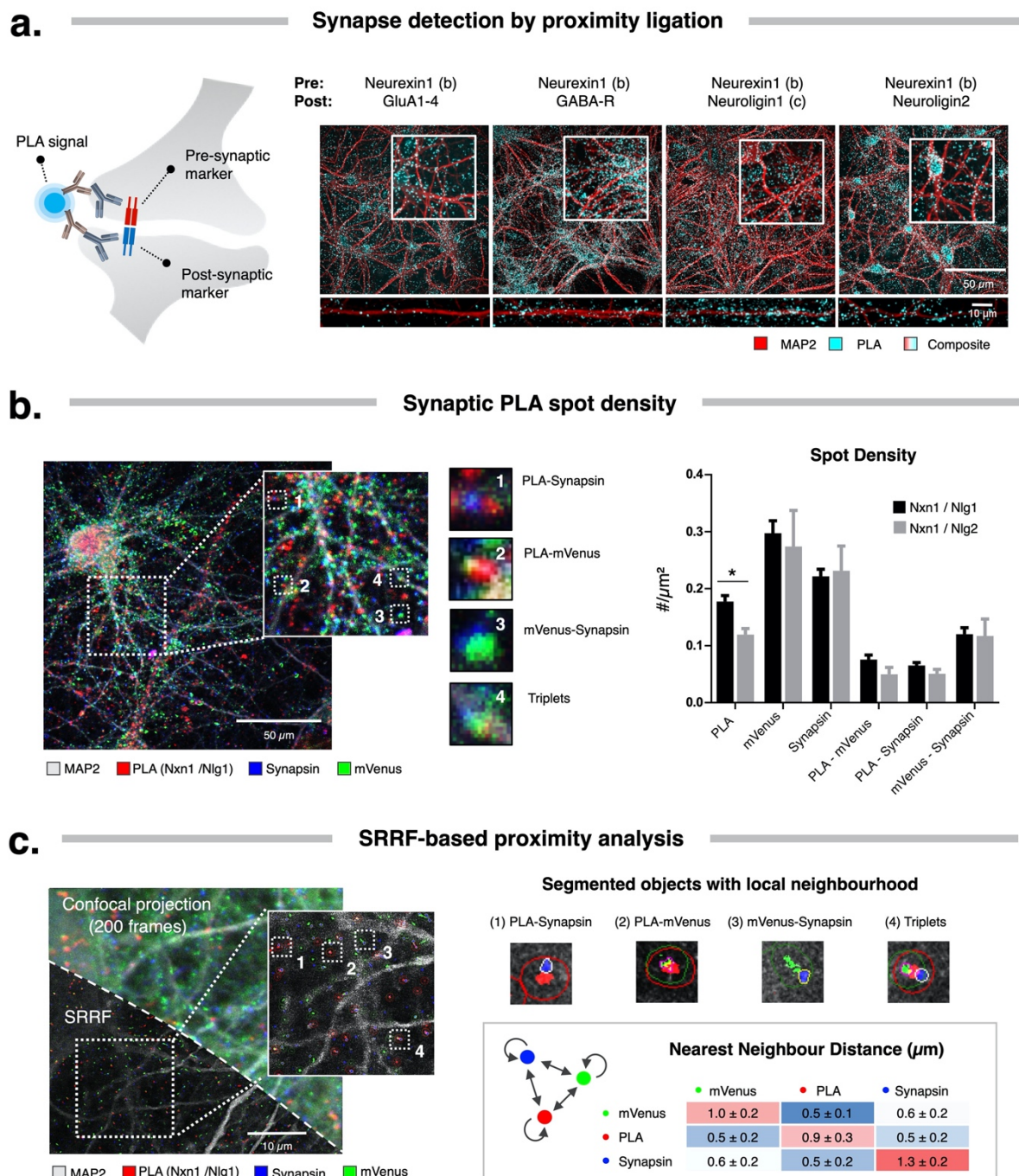
744

Figure 4. Proximity Ligation Assay for the detection and quantification of synapses. **a.** Diagram illustrating the principle of synaptic PLA (left) and representative images of synaptic PLA signal with the described combination of antibodies used in 14 DIV cortical neurons (right); **b.** Composite image of 28 DIV ENABLED cultures with synaptic PLA for Neurexin-Neuroligin1 and counterstained with MAP2 and Synapsin (triple stained), acquired with standard confocal microscopy. Insets show different types of combinations between synaptic PLA spots, mVenus

751   and Synapsin (center). The adjoined spot density quantification reveals differences between

752   individual markers, pairwise combinations and the PLA partners used (right); **c.** Maximum

753   intensity projection from a single confocal plane of triple stained cortical culture imaged 200

754   times (top half), overlaid with its superresolution result after application of SRRF (bottom half),

755   along with magnified insets. Nearest neighbor distances were calculated between all spots of

756   two markers, and the mean ± standard deviation is displayed per pairwise combination.
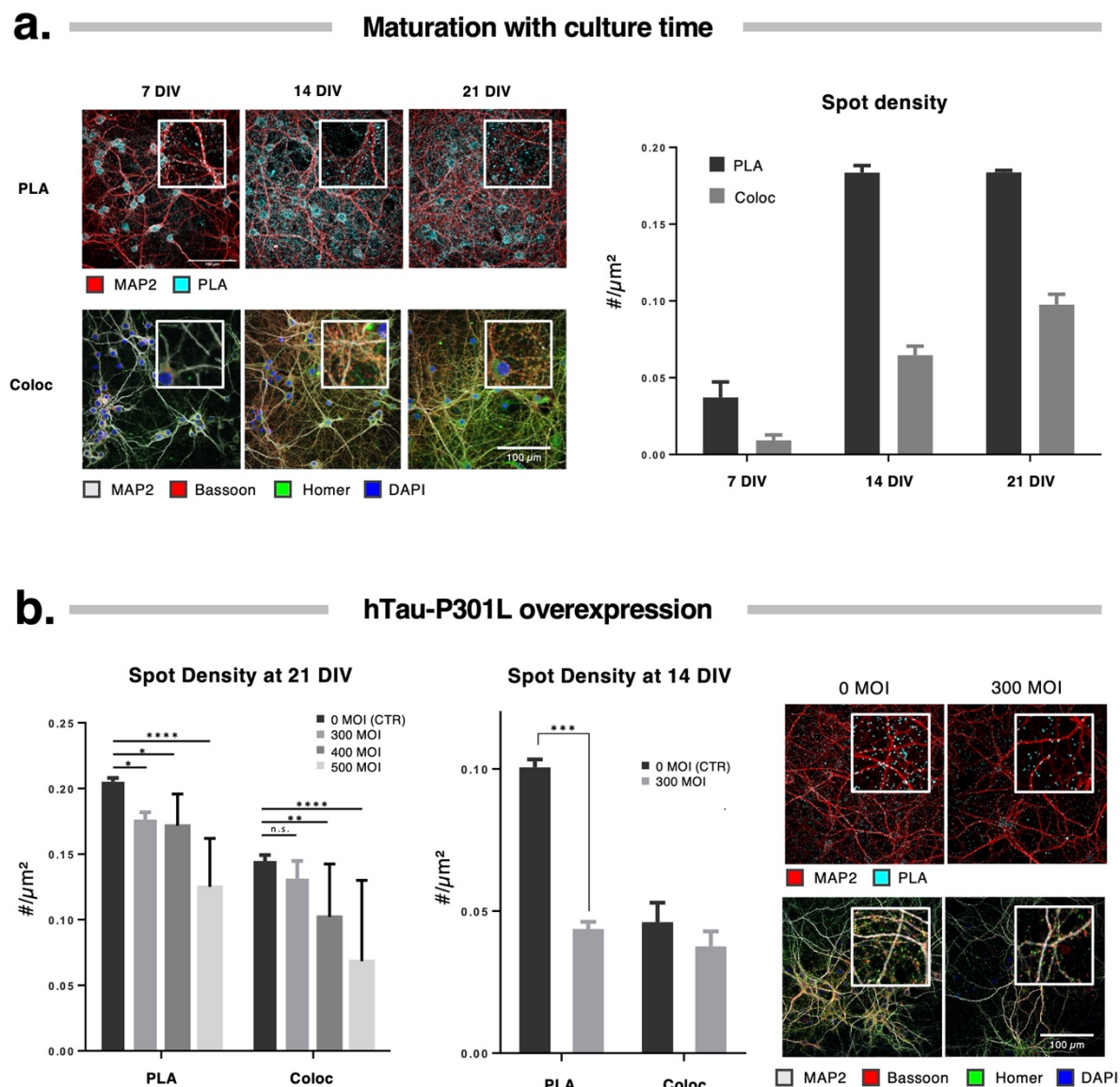
757

758

759

760

Figure 5. Synaptic PLA detects changes in synapse density in healthy and pathological conditions. **a.** Representative images (left) and quantification of spot density in cortical neuronal cultures at DIV 7, 14 and 21, after synaptic PLA (Neurexin/Neuroligin1) or colocalization (Bassoon/Homer); **b.** Quantification of synapse density after infection with a hTau.P301L AAV vector. Infection with different multiplicities of infection (300, 400 and 500 MOI), reveal a concentration-dependent effect at DIV 21, that is already significant for the lowest MOI when measured with PLA; **c.** Representative images (center) and quantification of neuronal cultures treated with hTau.P301L at 300 MOI revealing a significant effect synapse

770   density at 14 DIV. * = p-value < 0.05; **= p-value < 0.01; *** = p-value < 0.001, **** = p-

771   value < 0.0001, two-way ANOVA post-hoc Sidak's test.